Review

Effective tuning of the ratio of red to green emission of Ho^{3+} ions in single LiLuF$_4$ microparticle via codoping Ce^{3+} ions

CrossMark

Wei Gao*, Jun Dong, Jihong Liu, Xuewen Yan

School of Electronic Engineering, Xi'an University of Post & Telecommunications, Xi'an, 710121, PR China

ARTICLE INFO

ABSTRACT

Yb^{3+}/Ho^{3+} codoped LiLuF$_4$ microparticles have been successfully prepared via a facile hydrothermal method. The crystal phase and morphology of LiLuF$_4$ microparticles were inspected by x-ray diffraction and scanning electron microscope, respectively. The upconversion emission of single LiLuF$_4$: Yb^{3+}/Ho^{3+} microparticle was carefully studied by a confocal microscopy setup under NIR 980 nm excitation. With the increase of Ce^{3+} ion concentrations of 12%, the ratio of red to green emission of the Ho^{3+} ions of single LiLuF$_4$ microparticle was boosted about 17-fold, and the output colors were tuned from green to red, which is due to the two efficient cross-relaxation between Ho^{3+} and Ce^{3+} ions enhances the red and suppresses the green in the emission processes. To investigate the optical properties of the single microparticle or nanoparticle through the confocal microscopy setup can effectively avoid the influence of surrounding particle or environment, and could provide more precise information for better exploring the emission mechanisms of rare earth ions. The tunable upconversion emission of Ho^{3+} in single LiLuF$_4$ microparticle in this work will have great potential applications in the micro optoelectronic devices and color display applications.

© 2016 Elsevier B.V. All rights reserved.

Contents

1. Introduction

Upconversion (UC) emission of rare-earth-ion-doped fluoride nano- and micro-materials have been widely applied in phosphors, color displays, optical storages, solid-state lasers, solar cells and

biomedical imaging, which because of their low phonon energy (<350 cm^{-1}) can effectively suppress the nonradiative multiphonon relaxation processes [1–6]. Up to now, Many attempts have been made to synthesize UC fluoride nano- and micro-materials such as $NaYF_4$, $LiYF_4$, LaF_3, $NaScF_4$, etc. [7–10]. Especially, $NaYF_4$ crystals have been considered as one of the most efficient upconversion emission host matrix [11,12]. Recently, many researchers have reported that $NaLuF_4$ is a better host matrix for UC emission compared to the $NaYF_4$ [13–15]. Like $NaYF_4$ and $NaLuF_4$, tetragonal phase $LiYF_4$ crystal is also considered as an ideal matrix for trivalent rare earth ions [16,17]. It has been reported the total UC quantum yield of colloidal $LiYF_4$: Er^{3+} nanocrystals under 1490 nm excitation is almost 4 times higher than the hexagonal $NaYF_4$: Yb^{3+}/Er^{3+} nanocrystals [18]. With the same crystalline plane as $LiYF_4$, $LiLuF_4$ is a potentially efficient host material for UC emission, too. Chen's group has developed a unique strategy for the synthesis of novel $LiLuF_4$: Ln^{3+} core/shell UC nanoparticles with typically high absolute upconversion quantum yields, which have the great potential as efficient nanobioprobes in disease diagnosis [19]. However, to the best of our knowledge, tuning the UC emission properties of Ho^{3+} ions in single $LiLuF_4$ microparticle (MP) via codoping Ce^{3+} ions have been barely reported before. In this work, attempting to synthesize the tetragonal phase $LiLuF_4$: Yb^{3+}/Ho^{3+} MPs through a facile hydrothermal method. The structure and morphology of $LiLuF_4$ MPs were confirmed by x-ray diffraction (XRD) and the scanning electron microscope (SEM), respectively. We have tried to tune the ratio of red to green emission of Ho^{3+} in single $LiLuF_4$ MP through codoping Ce^{3+} ions under 980 nm excitation. The UC spectrum properties of single $LiLuF_4$: $Yb^{3+}/Ho^{3+}/Ce^{3+}$ MP were systematically studied by a confocal microscopy setup under NIR 980 nm excitation. The UC emission mechanisms between Ho^{3+} and Ce^{3+} ions were discussed based on emission spectrum.

2. Experimental

2.1. Materials

All chemicals used in the current study are analytical graded used without further purification. Lu_2O_3 (99.99%), $Yb(NO_3)_3 \cdot 5H_2O$ (99.99%), $Ho(NO_3)_3 \cdot 5H_2O$ (99.99%) and $Ce(NO_3)_3 \cdot 6H_2O$ (99.99%) are purchased from Sigma-Aldrich Chemicals Co. $Lu(NO_3)_3$ was prepared by dissolving the Lu_2O_3 in dilute nitric acid at elevated temperature followed by evaporating the superfluous nitric acid. NH_4F (98.0%), LiF (98.0%), and EDTA (ethylenediamine tetraacetic acid, 99.0%) with analytical grade are supplied by the Tianjin chemical reagent factory.

2.2. Synthesis of $LiLuF_4$: $Yb^{3+}/Ho^{3+}/Ce^{3+}$ MPs

A series of $LiLuF_4$:Yb^{3+}/Ho^{3+} MPs with codoping different Ce^{3+} ions were synthesized by a facile hydrothermal method [20]. In the preparation, firstly, 1.0 ml (1.00-x) ml $Lu(NO_3)_3$(0.5 M), 0.20 ml $Yb(NO_3)_3$(0.50 M), 0.02 ml $Ho(NO_3)_3$ (0.50 M), x ml($x = 0$, 0.04, 0.08, 0.12) $Ce(NO_3)_3$(0.50 M) and 20.0 ml EDTA(0.025 M) were slowly added into the solution under vigorous stirring 40 min. Secondly, 6.0 ml g NH_4F (0.50 M) and 4.0 ml g LiF (0.50 M) are added into the solution. Then stir it for about 20 min until it completely becomes white liquid. Finally, the mixture was slowly transferred into a 40.00 ml Teflon-lined autoclave and heated at 220 °C for 24 h. When the Telfon-line autoclave was cooled to room temperature, the samples were collected by centrifuging and washing with deionized water and ethanol 3–4 times, respectively. The collected $LiLuF_4$ MPs were obtained and dried at 60 °C for 12 h.

2.3. Sample characterization and spectral measurement

The structure and morphology of the samples were characterized by x-ray diffraction (XRD) with Cu Kα (40 kV, 40 mA) irradiation ($\lambda = 0.15406$ nm) and the scanning electron microscope (SEM, Quanta 200). The optical microscope (OLYMPUS-BX51) is used in the confocal setup, and the corresponding magnifications are 100, 500 and 1000. Ti sapphire laser (MBR-110, 700–1000 nm) and YAG: Nd^{3+} (Quanta Ray Lab-170, 10 Hz, 532 nm) pulse laser were employed as excitation sources. The spectrometer (SP2750i, 0.008 nm) with a PIXIS 100 charge coupled device (CCD, ACTON) and a PD471 photomultiplier tube (PMT, ACTON) were used for luminescence collection and detection. All of the spectroscopic measurements were carried out at room temperature.

3. Results and discussion

3.1. Structure and morphology

The typical XRD patterns of $LiLuF_4$: $20\%Yb^{3+}/2\%Ho^{3+}$ MPs with codoping different Ce^{3+} concentrations are given in Fig. 1. All the diffraction peaks from the four different products can be indexed as a pure tetragonal phase $LiLuF_4$, which coincides well with the standard pattern of JCPDS card 27-1251. No obvious extra diffraction peaks are detected even with increasing Ce^{3+} concentrations from 0% to 12%. In addition, it should be noticed that the diffraction peaks shifted slightly to the low angle side after Ce^{3+} doping. According to Bragg's law: $n\lambda = 2d \sin \theta$, d increases when θ decreases, which indicates the unit cell of $LiLuF_4$ expanded because Lu^{3+}
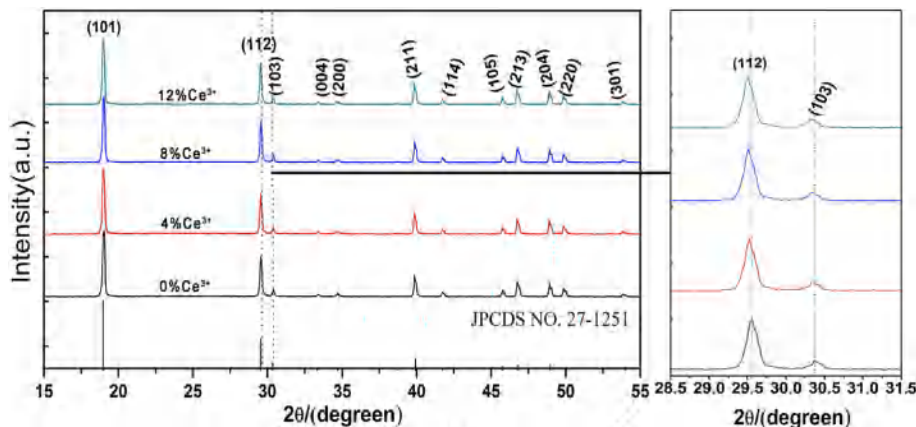
Fig. 1. XRD patterns of $LiLuF_4$: $20\%Yb^{3+}/2\%Ho^{3+}/xCe^{3+}$ MPs ($x = 0\%$, 4%, 8% and 12%).
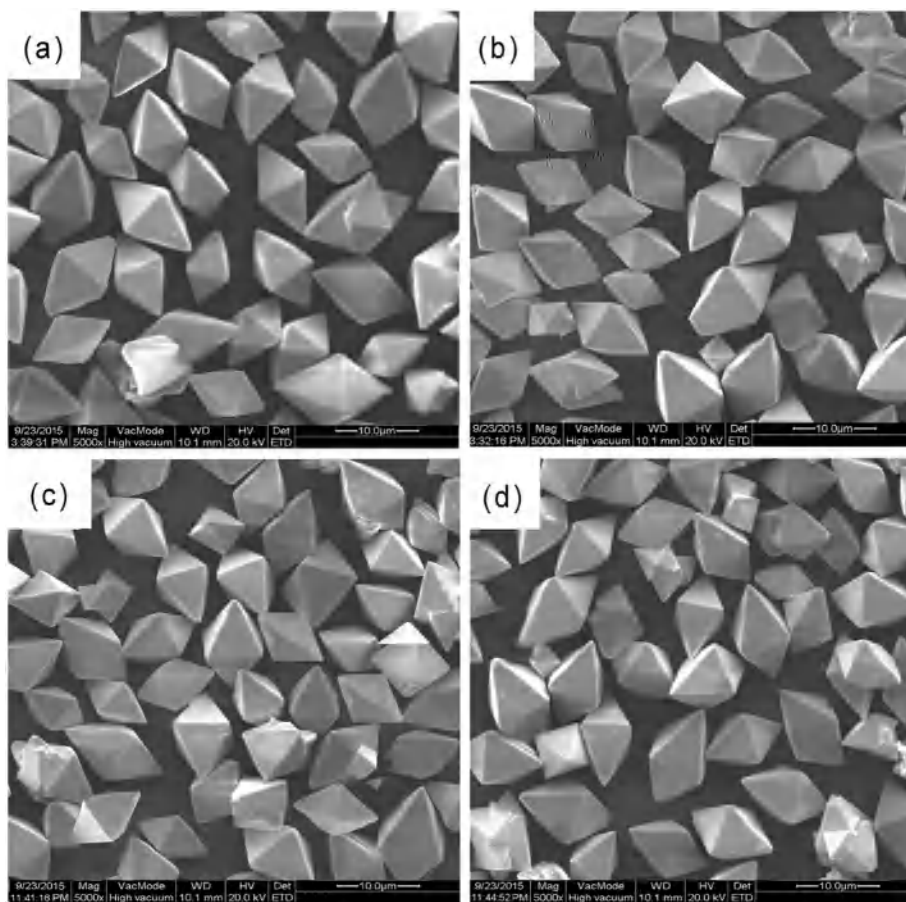
Fig. 2. SEM images of LiLuF$_4$: 20%Yb^{3+}/2%Ho^{3+} MPs with Ce^{3+} ions of 0%, 4%, 8% and 12%.

($r = 0.085$ nm) are substituted by bigger Ce^{3+} ($r = 0.128$ nm) in the host lattice [21,22].

Fig. 2 shows the SEM images of the LiLuF$_4$: Yb^{3+}/Ho^{3+} MPs with codoping different Ce^{3+} concentrations. A series of Ce^{3+} codoped LiLuF$_4$: Yb^{3+}/Ho^{3+} MPs display nearly octahedral in shape with a smooth surface, and the average size of the particles is around 10 μm. The morphology and size of LiLuF$_4$: Yb^{3+}/Ho^{3+} MPs have no obvious effect with increasing Ce^{3+} concentrations, which is due to a small amount of Ce^{3+} doping and the similar ionic radius between them. The analysis of EDX spectra indicates that the main elemental components of the samples are Lu, Yb, F, Ho and Ce, as shown in Fig. 3. The peak intensity of the Lu elemental is reduced when the introduction of Ce elemental in LiLuF$_4$: Yb^{3+}/Ho^{3+} NPs host lattice, which further indicates that Lu^{3+} occupy the lattice sites by the substitution of the Ce^{3+}.

3.2. UC emission of single LiLuF$_4$: Yb^{3+}/Ho^{3+} MP with codoping Ce^{3+} ions

The UC emission of single LiLuF$_4$: Yb^{3+}/Ho^{3+} MP with codoping Ce^{3+} ions is carefully investigated by a confocal microscopy system under NIR 980 nm excitation. The schematic diagram of the luminescence spectroscopy test system as shown in Fig. 4. Fig. 5 shows the UC emission spectra, the red-to-green(R/G) emission ratio and the Commission Internationale del'Eclairage (CIE) 1931 (x, y) chromaticity coordinates of single LiLuF$_4$: Yb^{3+}/Ho^{3+} MP with codoping Ce^{3+} ions, together with luminescence photographs. The two dominant emission peaks were clearly observed in single LiLuF$_4$: Yb^{3+}/Ho^{3+} MP, which can be assigned to the transitions of

$^5S_2/^5F_4 \rightarrow {}^5I_8$(center at 540 nm) and $^5F_5 \rightarrow {}^5I_8$(center at 650 nm) of Ho^{3+} ions in Fig. 5(a), respectively [23]. And they also exhibited weak NIR emission, which is associated with the transitions of $^5S_2/^5F_4 \rightarrow {}^5I_7$(center at 750 nm) of Ho^{3+} ions [23]. Interesting, with the Ce^{3+} concentrations increasing from 0% to 12% in single LiLuF$_4$: Yb^{3+}/Ho^{3+} MP, the red UC emission intensity increases and the green UC emission intensity decreases. The corresponding R/G ratio of Ho^{3+} is changed from 0.32 to 5.66, enhanced about 17-fold. The luminescent colors from single LiLuF$_4$: Yb^{3+}/Ho^{3+} MP can be tuned from green region to red region in the inset of Fig. 5(a) and (b). This result should be demonstrated according to the CIE chromaticity coordinate (x, y) as shown in Fig. 5(c), which is listed in Table 1.

3.3. UC mechanisms of single LiLuF$_4$: Yb^{3+}/Ho^{3+} MP with introducing Ce^{3+} ions

To understand the observed phenomenon, the UC emission mechanisms of the green and red are firstly studied. For unsaturated condition, the UC emission intensity (I_{up}) and infrared excitation pump power (P) can be described by the following relationship:$I_{up} \propto P^n$, where n is the number of pump photons required to populate the upper emitting state and its value can be obtained from the slope of the line in the plot of log(P) versus log(I_{up}) [24]. Fig. 6 shows the log−log plot of the UC emission intensities as a function of the infrared excitation pump power for single LiLuF$_4$: 20%Yb^{3+}/2%Ho^{3+} MP and single LiLuF$_4$:20%Yb^{3+}/2%Ho^{3+}/12%Ce^{3+} MP. The slopes of n for green and red emissions from single LiLuF$_4$: 20%Yb^{3+}/2%Ho^{3+} MP and single LiLuF$_4$: 20%Yb^{3+}/2%Ho^{3+}/12%Ce^{3+} MP are close to 2, which indicates that the green and red emissions
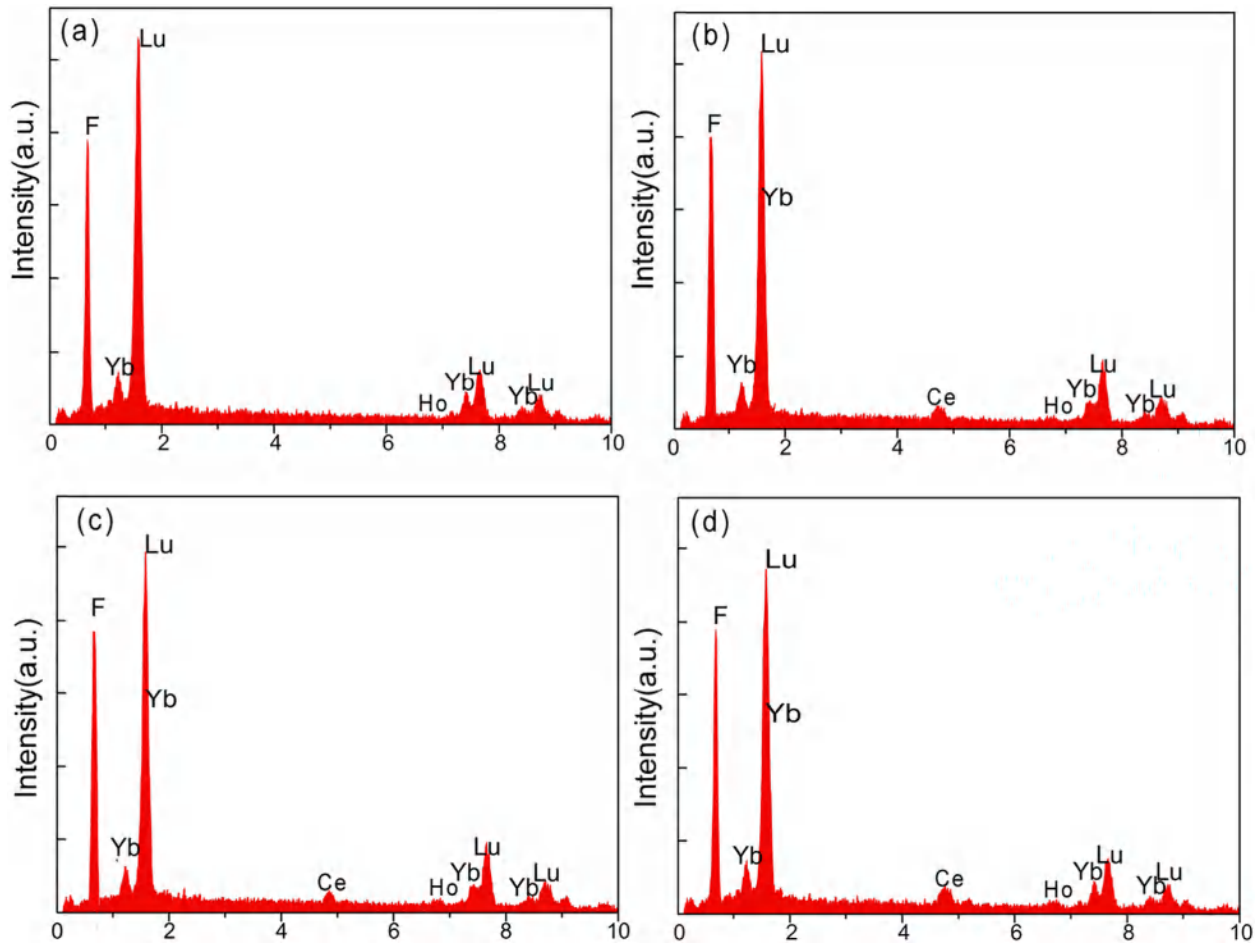
Fig. 3. EDX patterns of LiLuF$_4$: 20%Yb^{3+}/2%Ho^{3+} MPs with Ce^{3+} ions of 0%, 4%, 8% and 12%.

are two photon excitation processes [25]. Noticed that the slopes of n from single LiLuF$_4$: 20%Yb^{3+}/2%Ho^{3+}/12%Ce^{3+} MP are slightly smaller than that single LiLuF$_4$: 20%Yb^{3+}/2%Ho^{3+} MP, which was mainly attributed to the change of population of the red intermediate level due to the quenching of the green UC emissions [26].

To further explore the influence of Ce^{3+} on the emission of Ho^{3+}, the main processes of radiative transition and processes for UC emission in single LiLuF$_4$ MCs should be discussed based on the

emission spectra. Fig. 7 illustrates a possible scheme of UC emission processes of Yb^{3+}/Ho^{3+}/Ce^{3+} system [27]. Under NIR 980 nm excitation, the main pathway to populate excited states of Ho^{3+} is through the three successive energy transfer (ET) from Yb^{3+} to Ho^{3+}, which because Yb^{3+} has a larger absorption cross-section for infrared light and longer excited state lifetime than Ho^{3+}. The excited state $^5I_6$, $^5F_5$ and $^5S_2/^5F_4$ of Ho^{3+} can be populated by ET processes from neighboring Yb^{3+}. When the excited state $^5S_2/^5F_4$
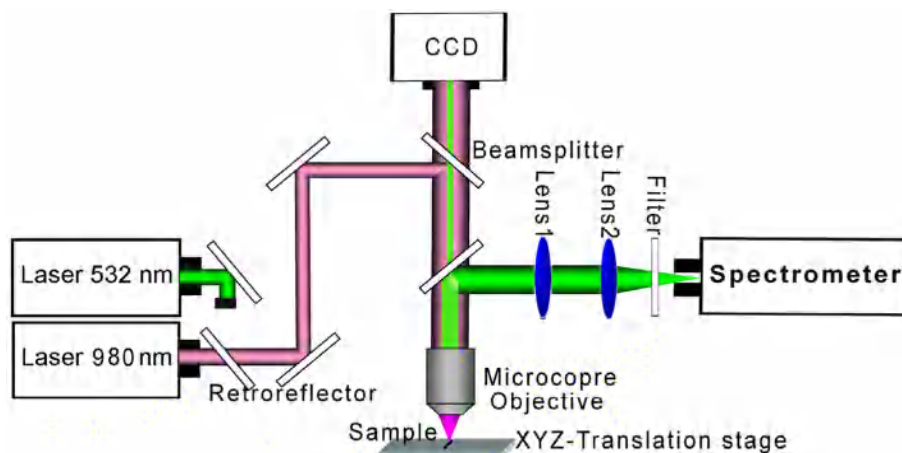
Fig. 4. Schematic diagram of luminescence spectroscopy test system.
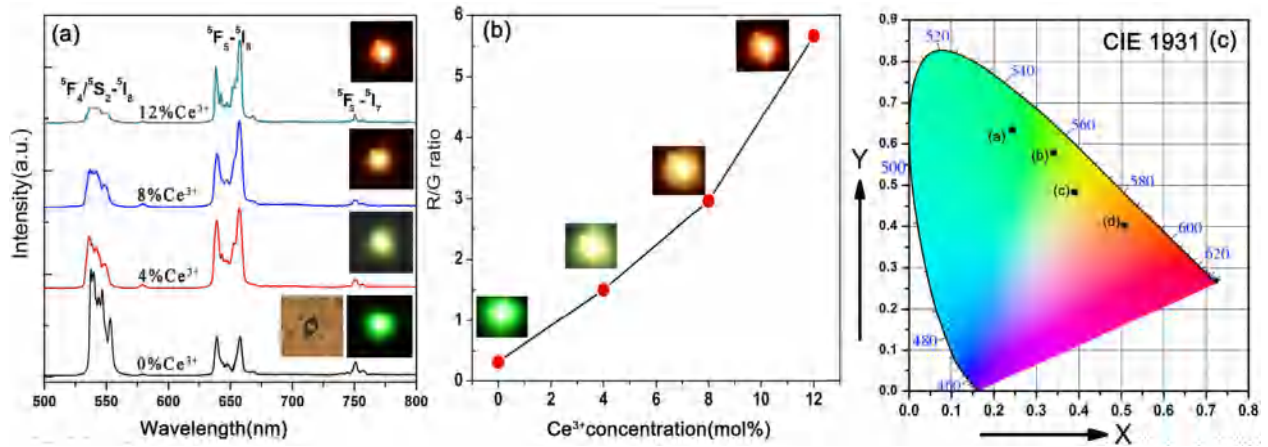
Fig. 5. (a) UC emission spectra, (b) R/G ratio, (c) CIE diagram of single LiLuF$_4$: Yb^{3+}/Ho^{3+}/Ce^{3+} MP for different Ce^{3+} ion concentration under 980 nm excitation. The inset is corresponding luminescence photographs.

Table 1
The calculated CIE chromaticity coordinates (x, y) of single LiLuF$_4$: Yb^{3+}/Ho^{3+} MCs with different Ce^{3+} concentrations.

Point	Samples	CIE chromaticity coordinates	
		x	y
a	LiLuF$_4$: 20%Yb^{3+}/2%Ho^{3+}	0.2431	0.6314
b	LiLuF$_4$: 20%Yb^{3+}/2%Ho^{3+}/4%Ce^{3+}	0.3389	0.5642
c	LiLuF$_4$: 20%Yb^{3+}/2%Ho^{3+}/6%Ce^{3+}	0.4202	0.4713
d	LiLuF$_4$: 20%Yb^{3+}/2%Ho^{3+}/8%Ce^{3+}	0.5274	0.3628
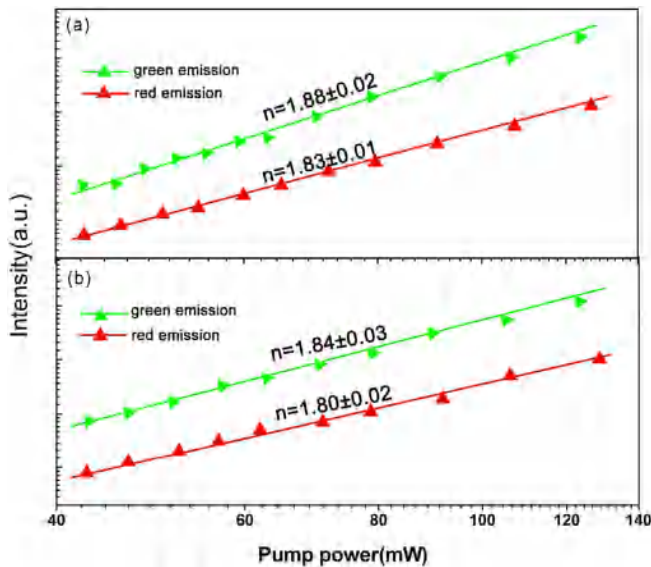
Fig. 6. Pump power dependence of single LiLuF$_4$: 20%Yb^{3+}/2%Ho^{3+}/xCe^{3+} MCs (x = 0% (a) and 12% (b)).

and $^5F_5$ radiative decay to the ground state $^5I_8$, the green and red UC emissions can be generated. The red UC emission mainly originates from excited state $^5F_5$, and it can be populated through two possible transition processes. One is the direct population from the nonradiative transition from the excited state $^5F_4/^5S_2$ of Ho^{3+}. The other is from $^5I_7$ to $^5F_5$ state by through the ET process from Yb^{3+} to Ho^{3+}, and $^5I_7$ state can be populated through the nonradiative relaxation from the $^5I_6$ state. Thus, red UC emission

intensity of Ho^{3+} mainly depends on the two nonradiative relaxation processes originate from $^5S_2/^5F_4 \rightarrow ^5F_5$ and $^5I_6 \rightarrow ^5I_7$ transitions. However, according to multiphonon nonradiative relaxation rate $W_{NR} = A \exp^{-BP}$, here, A and B are host constants, $P = \Delta E/h\nu$ is the number of phonons involved, ΔE is the energy gap between two energy levels and $h\nu$ is the highest-energy vibrational mode of the host lattice [28]. Generally speaking, when the doped ion concentration is low, the ion interaction can be ignored. The multiphonon nonradiative transition rate is mainly decided by the maximum phonon energy of the host lattice [29]. Usually, the multiphonon nonradiative relaxations process dominates over radiative process when the P is less than 5. Since both energy gaps of $^5S_2/^5F_4 \rightarrow ^5F_5$ and $^5I_6 \rightarrow ^5I_7$ are about 3000 cm^{-1}, which is approximately 6 times higher than that the maximum phonon energy of LiLuF$_4$ is less than 500 cm^{-1} [30,31]. Consequently, the UC emission from Yb^{3+} and Ho^{3+} codoped system usually exhibit intense green emission accompanied by weak red emission, which because of the two inefficient nonradiative process of $^5S_2/^5F_4 \rightarrow ^5F_5$ and $^5I_6 \rightarrow ^5I_7$ transition [32].

However, when Ce^{3+} is introduced to the LiLuF$_4$: 20%Yb^{3+}/2% Ho^{3+} system, the more high R/G ratio is observed as shown in Fig. 4(b). One can find that the R/G ratio is enhanced 17-fold in single LiLuF$_4$: 20%Yb^{3+}/2%Ho^{3+} MP and luminescent colors of Ho^{3+} is tuned from green to red and when the Ce^{3+} concentration is increased to 12%. Since the energy gap between the excited state $^5F_{7/2}$ and ground state $^2F_{5/2}$ is about 3000 cm^{-1} of Ce^{3+} ions is similar to the energy gaps of $^5S_2/^5F_4 \rightarrow ^5F_5$ and $^5I_6 \rightarrow ^5I_7$ transitions of Ho^{3+} [33]. The two inefficient nonradiative processes of $^5S_2/^5F_4 \rightarrow ^5F_5$ and $^5I_6 \rightarrow ^5I_7$ transitions of Ho^{3+} can be replaced in order by cross relaxation (CR) processes of $^5S_2(^5F_4)$ (Ho^{3+}) + $^2F_{5/2}$ (Ce^{3+}) $\rightarrow ^5F_5$ (Ho^{3+}) + $^2F_{7/2}$ (Ce^{3+}) and $^5I_6$ (Ho^{3+}) + $^2F_{5/2}$ (Ce^{3+}) $\rightarrow ^5I_7$ (Ho^{3+}) + $^2F_{7/2}$ (Ce^{3+}) between Ho^{3+} and Ce^{3+} ions, which can efficiently increase the populations of $^5F_5$ state, resulting in the enhancement of red emission and the suppress of green emission.

3.4. The further identification of the occurrence of CR processes

In order to further confirm the occurrence of CR processes between Ho^{3+} and Ce^{3+} ions. More results of the experiment about CR processes are carefully investigated. Fig. 8(a) shows NIR (1175 nm) emission of $^5I_6 \rightarrow ^5I_8$ transition of Ho^{3+} ions in single LiLuF$_4$: Yb^{3+}/Ho^{3+} MP with codoping different Ce^{3+} ion concentrations under 980 nm excitation. The relative intensity of NIR emission of $^5I_6 \rightarrow ^5I_8$ transition decreases after the Ce^{3+}
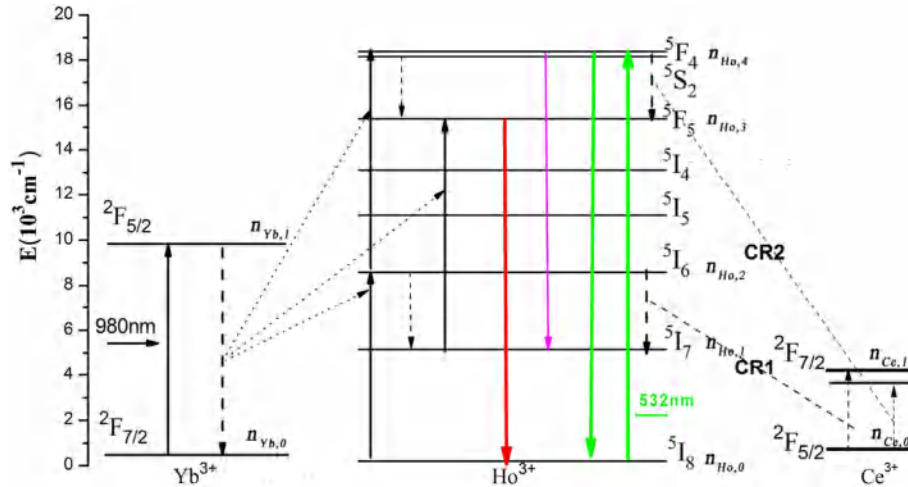
Fig. 7. Energy level diagrams of Ho^{3+}, Yb^{3+} and Ce^{3+} ions as well as proposed UC mechanisms.
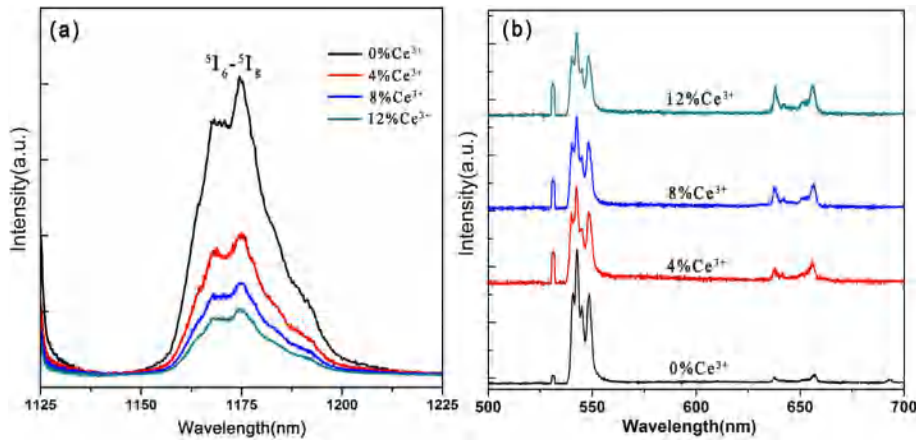
Fig. 8. (a) The NIR spectra of $^5I_6 \rightarrow {}^5I_8$ transition and (b) the DC emission of Ho^{3+} of single $LiLuF_4$: $20\%Yb^{3+}/2\%Ho^{3+}$ MP with codoping different Ce^{3+} ion concentrations under 980 nm and pulse laser 532 nm excitation, respectively.

concentration increase from 0% to 12.0%. It is well known that the fluorescence emission intensity mainly ascribes to the competition between radiative relaxation and nonradiative relaxation. The intensity of NIR emission decreases indicates that nonradiative decay rate from $^5I_6$ state have been increased with the increase of Ce^{3+} concentrations, which deduces the occurrence of CR1 process $^5I_6$ (Ho^{3+}) + $^2F_{5/2}$ (Ce^{3+}) $\rightarrow {}^5I_7$ (Ho^{3+}) + $^2F_{7/2}$(Ce^{3+}) between Ho^{3+} and Ce^{3+} ions.

The downconversion (DC) emission from $^5S_2/^5F_4 \rightarrow {}^5I_8$ transition of Ho^{3+} in single $LiLuF_4$: Yb^{3+}/Ho^{3+} MPs under 532 nm pulsed laser excitation, as shown in Fig. 8(b). The $^5S_2/^5F_4$ excited states can be directly populated by 532 nm pulsed laser, and generates green emission by radiative decay from $^5S_2/^5F_4 \rightarrow {}^5I_8$ transition in Fig. 5. The red emission mainly originates from $^5F_5$ state. Noted that the green emission intensity reduces and red emission increases with the increase of Ce^{3+} ion concentrations, and the corresponding R/G ratio is enhanced from 0.12 to 0.76. According to the above discussion, the nonradiative process of $^5S_2/^5F_4 \rightarrow {}^5F_5$ transition is inefficient. Therefore, the more high R/G ratio of single $LiLuF_4$: Yb^{3+}/Ho^{3+} MP can be obtained, which further indicate that the occurrence of CR2 process of $^5S_2/^5F_4$ (Ho^{3+}) + $^2F_{5/2}$ (Ce^{3+}) $\rightarrow {}^5F_5$ (Ho^{3+}) + $^2F_{7/2}$ (Ce^{3+}) between Ho^{3+} and Ce^{3+}.

3.5. The conversion efficiency of CR 1 and CR 2 processes

The conversion efficiency of CR processes between Ho^{3+} and Ce^{3+} can be calculated based on the steady-state rate equations and decay lifetime. $n_{Ho,0}$, $n_{Ho,1}$, $n_{Ho,2}$, $n_{Ho,3}$ and $n_{Ho,4}$ represent the population densities of the $^5I_8$, $^5I_7$, $^5I_6$, $^5F_5$ and $^5S_2(^5F_4)$ states of the Ho^{3+} ions, respectively; $n_{Ce,0}$ and $n_{Ce,1}$, $n_{Yb,0}$ and $n_{Yb,1}$ are the population densities of the $^2F_{5/2}$ and $^2F_{7/2}$ levels of the Ce^{3+} ions and the $^2F_{7/2}$ and $^2F_{5/2}$ levels of the Yb^{3+} ions, respectively; E_0, E_1 and E_2 are ET rates from the Yb^{3+} ions to Ho^{3+} ions, respectively; r_1, r_2, r_3 and r_4 are the intrinsic decay rates from the $^5I_7$, $^5I_6$, $^5F_5$ and $^5S_2(^5F_4)$ of the Ho^{3+} ions, respectively; C_1 and C_2 are the ET rate for Ho^{3+} to Ce^{3+} CR process, respectively. β_0 and β_1 refer to nonradiative decay rates from $^5I_6 \rightarrow {}^5I_7$ and $^5S_2/^5F_4 \rightarrow {}^5F_5$ states, respectively. Considering that the radiative relaxation probability of the $^5I_5$ and $^5I_4$ states is very low due to the small neighbored energy gap, we ignore the terms of radiation rates in the rate equations. In the case of continuous wave laser excitation, the rate equations of each energy states are formulated as follows [34,35]:

$$\beta_0 n_{Ho,2} + C_1 n_{Ho,2} n_{Ce,0} - r_1 n_{Ho,1} - E_1 n_{Yb,1} n_{Ho,1} = 0 \qquad (1a)$$
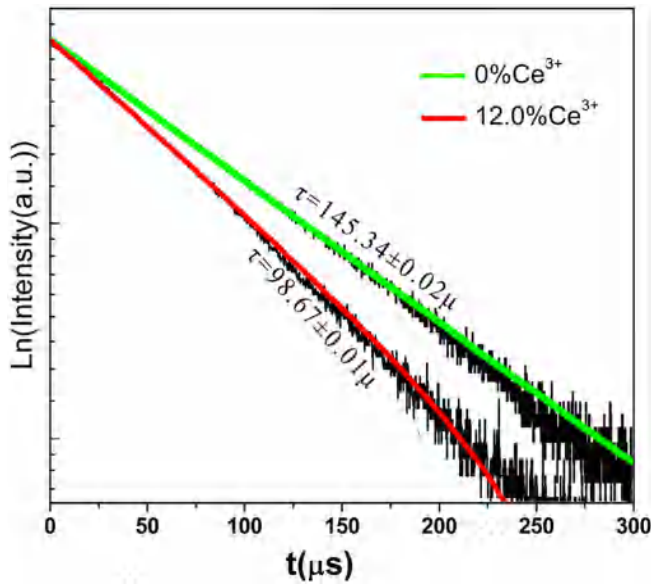
Fig. 9. DC luminescence decays of $^5S_2/^5F_4 \rightarrow {}^5I_8$ transition at 541 nm of Ho^{3+} for single $LiLuF_4$: $20\%Yb^{3+}/2\%Ho^{3+}/xCe^{3+}$ NCs (x = 0% and 12%). The luminescence decay curves are fitted by using a single exponential function.

$$E_0 n_{Yb1} n_{Ho,0} - \beta_0 n_{Ho,2} - C_1 n_{Ho,2} n_{Ce,0} - r_2 n_{Ho,2} - E_2 n_{Yb,1} n_{Ho,1}$$
$$= 0 \tag{1b}$$

$$E_1 n_{Yb,1} n_{Ho,1} + C_2 n_{Ho,4} n_{Ce,0} + \beta_1 n_{Ho,4} - r_3 n_{Ho,3} = 0 \tag{1c}$$

$$E_2 n_{Yb,1} n_{Ho,2} - r_4 n_{Ho,4} - \beta_1 n_{Ho,4} - C_2 n_{Ho,4} n_{Ce,0} = 0 \tag{1d}$$

Generally, the intrinsic decay rates at the intermediate states are much larger than the UC ET rates [24]. one can estimate the emission intensity of NIR ($^5I_6 \rightarrow {}^5I_8$) the of the Ho^{3+} ions according to the following equations (1a)-(1d):

$$I_{NIR} = n_{Ho,2} h\nu_{NIR} r_2 = \frac{r_2}{r_2 + C_1 n_{Ce0}} h\nu_{NIR} E_1 n_{Ho,0} n_{Yb,1} \tag{2}$$

Based on the measured fluorescence intensity in Fig. 8(a) and equation (2), we have

$$\frac{I_{NIR}(0\%Ce)}{I_{NIR}(12.0\%Ce)} = \frac{r_2 + C_1 n_{Ce,0}}{r_2} = 1 + \frac{C_1 n_{Ce,0}}{r_2} = 4.61 \tag{3}$$

The conversion efficiency of the CR1 process [36]:

$$\eta_1 = \frac{\beta_1 + C_1 n_{Ce,0}}{r_2 + C_1 n_{Ce,0}} \approx \frac{1}{\frac{r_2}{C_1 n_{Ce,0}} + 1} = 78.3\% \tag{4}$$

The conversion efficiency of CR2 process can be calculated with the following equation [4]:

$$\eta_2 = 1 - \frac{\tau(12\%Ce)}{\tau(0\%Ce)} = 32.1\% \tag{5}$$

Fig. 9 shows the luminescence decay curves are fitted by using a single exponential function. The corresponding conversion efficiency of CR1 and CR2 has been calculated to be about 78.3% and 32.1%, respectively. This result indicates that the CR2 plays the assistant role for the CR1 process to covert the green UC emission into red UC emission.

4. Conclusions

The pure tetragonal phase $LiLuF_4$: Yb^{3+}/Ho^{3+} MCs have been successfully synthesized by a facile hydrothermal method. The UC emission of single $LiLuF_4$: Yb^{3+}/Ho^{3+} MCs with codoping Ce^{3+} ion was carefully investigated with a confocal microscopy setup under NIR 980 nm excitation. The R/G ratio of single $LiLuF_4$: Yb^{3+}/Ho^{3+} MCs is effectively boosted 17-fold with the Ce^{3+} concentrations are increased to 12%, which is mainly due to the two nonradiative transitions of $^5S_2/^5F_4 \rightarrow {}^5F_5$ and $^5I_6 \rightarrow {}^5I_7$ are substituted in order by the two efficient CR processes of $^5S_2/^5F_4$ (Ho^{3+}) + $^2F_{5/2}$ (Ce^{3+}) $\rightarrow {}^5F_5$ (Ho^{3+}) + $^2F_{7/2}$ (Ce^{3+}) and $^5I_6$ (Ho^{3+}) + $^2F_{5/2}$ (Ce^{3+}) $\rightarrow {}^5I_7$ (Ho^{3+}) + $^2F_{7/2}$(Ce^{3+}) between Ho^{3+} and Ce^{3+}, respectively. The more high R/G ratio of Ho^{3+} in single $LiLuF_4$ MCs mainly depends on CR1 process according to the calculated conversion efficiency. The present study is of great importance in the multicolor tuning of RE doped micro-materials as well as extending their applications in micro optoelectronic devices and color display applications.

References

[1] N. Menyuk, K. Dwight, F. Pinaud, Appl. Phys. Lett. 21 (1972) 159–161.
[2] M. Stockman, Nat. Mater 3 (2004) 423–424.
[3] P. Cheben, F. Monte, D. Worsfold, D. Carlsson, C. Grover, J. Mackenzie, Nature 408 (2000) 64–67.
[4] G. Rumbles, Nature 409 (2001) 572–573.
[5] X. Huang, S. Han, W. Huang, X.G. Liu, Chem. Soc. Rev. 42 (2013) 173–201.
[6] M.E. Lim, Y.L. Lee, Y. Zhang, J.J.H. Chu, Biomaterials 33 (2012) 1912–1920.
[7] M.Y. Ding, S.L. Yin, Y.R. Ni, C.H. Lu, D.Q. Chen, J.S. Zhong, Z.G. Ji, Z.Z. Xu, Ceram. Int. 41 (2015) 7411–7420.
[8] N. Martin, P. Boutinaud, M. Malinowski, R. Mahion, J.C. Cousseins, J. Alloys Compd. 304 (1998) 275–277.
[9] H.X. Mai, Y.W. Zhang, R. Si, Z.G. Yan, L.D. Sun, L.P. You, C.H. Yan, J. Am. Chem. Soc. 128 (2006), 6426–64369.
[10] Y. Wei, F.Q. Lu, X.R. Zhang, D.P. Chen, Chem. Mater 18 (2006) 5733–5737.
[11] S. Heer, K. Kompe, H.U. Gudel, M. Haase, Adv. Mater 16 (2004) 2012–2015.
[12] H.X. Mai, Y.W. Zhang, L.D. Sun, C.H. Yan, J. Phys. Chem. C 111 (2007) 13721–13729.
[13] S.J. Zeng, J.J. Xiao, Q.B. Yang, J.H. Hao, J. Mater. Chem. 22 (2012) 9870–9874.
[14] Q. Liu, Y. Sun, T.S. Yang, W. Feng, C.G. Li, F.Y. Li, J. Am. Chem. Soc. 133 (2011) 17122–17125.
[15] L.L. Wang, M. Lan, Z.Y. Liu, G.S. Qin, C.F. Wu, X. Wang, W.P. Qin, W. Huang, L. Huang, J. Mater. Chem. C 1 (2013) 2485–2490.
[16] K. Ogasawara, S. Watanabe, H. Toyoshima, T.M.G. Ishii, B.H. Ikeno, I.J. Tanaka, Solid. State.Chem. 178 (2005) 412.
[17] X.J. Pei, Y.B. Hou, S.L. Zhao, Z. Xu, F. Teng, Mater. Chem Phys. 90 (2005) 270–274.
[18] G.Y. Chen, T.Y. Ohulchanskyy, A. Kachynski, H. Ågren, P.N. Prasad, ACSNANO 5 (2011) 4981–4986.
[19] P. Huang, W. Zheng, S.Y. Zhou, D.T. Tu, Z. Chen, H.M. Zhu, R.F. Li, E. Ma, M.D. Huang, X.Y. Chen, Angew. Chem. Int. Ed. 53 (2014) 1252–1257.
[20] J. Li, H.R. Zheng, W. Gao, E.J. He, D.L. Gao, Y. Tian, Chin. Sci. Bull. 57 (2012) 2366–2369.
[21] R.D. Shannon, Acta Crystallogr. A 32 (1976) 751–767.
[22] Q.Q. Dou, Y. Zhang, Langmuir 27 (2011) 13236–13241.
[23] G.D. Gilliland, R.C. Powell, Phys. Rev. B 38 (1988) 9958–9973.
[24] M. Pollnau, D.R. Gamelin, S.R. Lüthi, H.U. Güdel, M.P. Hehlen, Phys. Rev. B 61 (2000) 3337–3346.
[25] L.W. Yang, H.L. Han, Y.Y. Zhang, J.X. Zhong, J. Phys. Chem. C 113 (2009) 18995–18999.
[26] G.Y. Chen, H.C. Liu, G. Somesfalean, H.J. Liang, Z.G. Zhang, Nanotechnology 20 (2009) 385704.
[27] N.M. Sangeha, F.C.J.M. van Veggel, J. Phys. Chem. C 113 (2009) 14702–14707.
[28] T. Schmidt, G. Müller, L. Spanhel, Chem. Mater 10 (1998) 65–71.
[29] R. Monika, K.S. Sunil, K.S. Akhilesh, P. Ritika, K. Biplob, M. Kavita, B.R. Shyam,

ACS Appl. Mater. Interfaces 7 (2015) 15339−15350.

[30] D.R. Gamelin, H.U. Gudel, Top. Curr. Chem. 214 (2001) 1−55.
[31] T. Li, C.F. Guo, Y.M. Yang, N. Zhang, L. Li, Acta Mater 61 (2013) 7481−7487.
[32] W. Wei, Y. Zhang, R. Chen, J.L. Goggi, N. Ren, L.g Huang, K.K. Bhakoo, H.D. Sun, T.T.Y. Tan, Chem. Mater 26 (2014) 5183−5186.
[33] Y.C. Li, L.W. Yang, Y. Li, S.X. Yu, P. Yang, F. Jiang, Ceram. Int. 39 (2013) 1183−1188.
[34] G.Y. Chen, H.C. Liu, G. Somesfalean, H.J. Liang, Z.G. Zhang, Nanotechnology 20 (2009) 385704.
[35] R.R. Deng, F. Qin, R.F. Chen, W. Huang, M.H. Hong, X.G. Liu, Nature 10 (2015) 237−242.
[36] E. De la Rosa, P. Salas, H. Desirena, C. Angeles, R.A. Rodríguez, Appl. Phys. Lett. 87 (2005), 241912-1−;24191−2.